AMERICAN SOCIETY FOR MICROBIOLOGY | Journal of Virology®

PATHOGENESIS AND IMMUNITY

The Furin-S2′ Site in Avian Coronavirus Plays a Key Role in Central Nervous System Damage Progression

Jinlong Cheng,[a] Ye Zhao,[a] Yanxin Hu,[a] Jing Zhao,[a] Jia Xue,[a] Guozhong Zhang[a]

[a]Key Laboratory of Animal Epidemiology of the Ministry of Agriculture, College of Veterinary Medicine, China Agricultural University, Beijing, People's Republic of China

ABSTRACT The furin cleavage site plays an important role in virus pathogenicity. The spike protein of severe acute respiratory syndrome coronavirus 2 (SARS-CoV-2) harbors a furin cleavage site insertion, in contrast to SARS-CoV, which may be related to its stronger communicability. An avian coronavirus with an extra furin cleavage site upstream of the fusion peptide (furin-S2′ site) infected monocytes and neuron cells, leading to viremia and encephalitis, respectively. Immunohistochemistry and real-time quantitative PCR were used to follow disease progression and demonstrated differences between the parent avian coronavirus and mutated avian coronavirus with a furin-S2′ site. Magnetic resonance imaging and biological dye to evaluate the blood-brain barrier permeability showed that avian coronavirus with a furin-S2′ site had increased permeability compared with that of the parent avian coronavirus. Immunohistochemistry of brains after intracerebral injection of avian coronavirus and immunofluorescence staining of primary neuron cells demonstrated that the furin-S2′ site expanded the cell tropism of the mutant avian coronavirus to neuron cells. Tumor necrosis factor alpha (TNF-α), which has a key role in blood-brain barrier permeability, was highly induced by avian coronavirus with a furin-S2′ site in comparison with the parent avian coronavirus. We demonstrated the process involved in mutant avian coronavirus-induced disease and that the addition of a furin-S2′ site changed the virus cell tropism.

IMPORTANCE Coronaviruses have broken out three times in 2 decades. Spike (S) protein plays a key role in the process of infection. To clarify the importance of the furin cleavage site in spike protein for coronavirus, we investigated the pathogenesis of neurotropic avian coronavirus, whose spike protein contains an extra furin cleavage site (furin-S2′ site). By combining real-time quantitative PCR and immunohistochemistry, we demonstrated that infectious bronchitis virus (IBV) infects brain instead of trachea when its S protein contains the furin-S2′ site. Moreover, the virus was shown to increase the permeability of the blood-brain barrier, infect neuron cells, and induce high expression of TNF-α. Based on these results, we further showed that the furin cleavage site in S protein plays an important role in coronavirus pathogenicity and cell tropism. Our study extends previous publications on the function of S protein of coronavirus, increasing researchers' understanding of coronavirus.

KEYWORDS coronavirus, furin-S2′ site, cell tropism, blood-brain barrier, TNF-α

Coronaviruses (CoVs) are enveloped, single-strand-positive RNA viruses belonging to the order *Nidovirales* which infect epithelial cells and are mostly responsible for respiratory and digestive tract disease in humans and animals. Human CoV 229E (HCoV-229E) is the main cause of the common cold, while severe acute respiratory syndrome coronavirus (SARS-CoV), Middle East respiratory syndrome coronavirus (MERS-CoV), and SARS-CoV-2 cause severe respiratory disease that can be life-threatening to humans (1–5). Other CoVs, including hepatitis virus John Howard Mueller strain (MHV-JHM), human coronavirus OC43 (HCoV-OC43), and porcine hemagglutinating encephalomyelitis virus (PHEV), can damage the central nervous system (CNS), causing

Citation Cheng J, Zhao Y, Hu Y, Zhao J, Xue J, Zhang G. 2021. The furin-S2′ site in avian coronavirus plays a key role in central nervous system damage progression. J Virol 95:e02447-20. https://doi.org/10.1128/JVI.02447-20.

Editor Mark T. Heise, University of North Carolina at Chapel Hill

Address correspondence to Guozhong Zhang, zhanggz@cau.edu.cn.

Received 23 December 2020
Accepted 10 March 2021
Accepted manuscript posted online 16 March 2021
Published 10 May 2021

encephalitis (6–8). According to recent studies, SARS-CoV-2 can cause CNS manifestations such as acute cerebrovascular disease, ataxia, and seizure as well as peripheral nervous system (PNS) manifestations such as olfactory and gustatory disturbances (9–13). Infectious bronchitis virus (IBV), an avian coronavirus, belongs to the gamma coronavirus group (γ-CoV), which causes a highly contagious, acute viral respiratory disease in chickens, and has caused great economic losses in the poultry industry. Currently, QX-type IBV is epidemic worldwide, and it has been reported to damage the respiratory, digestive, and urogenital systems of chickens (14, 15).

IBV, similar to other coronaviruses, encodes four structural proteins: spike glycoprotein (S), small envelope protein (E), membrane glycoprotein (M), and nucleocapsid proteins (N) (16). The S protein, an important surface protein, plays a key role in infection. IBV attaches to cell surface receptors via the S protein and invades the cell via the clathrin-mediated endosomal pathway, where viral membrane fusion occurs (17). S protein is typically cleaved by a host cell furin-like protease into two separate polypeptides named S1 and S2 subunits. While S1 is a large receptor-binding domain, S2 harbors a fusion peptide (FP), heptad repeat domains, and transmembrane domain (18). There is an extra furin cleavage site (FCS) (furin-S2′ site) upstream of the fusion peptide in the S2 subunit of some CoVs, which was reported to influence invasion. In the IBV Beaudette strain, the furin-S2′ site is a determinant of cellular adaption; the Beaudette strain does not grow in the Vero cell line without a furin-S2′ site (19). When the original sequence PTKR/S of SARS-CoV was replaced with RRKR/S, SARS-CoV could invade susceptible cells independently of cathepsin L (20). Unlike SARS-CoV, the furin cleavage site insertion in SARS-CoV-2 is essential for its ability to infect human lung cells and might be related to its stronger communicability (21, 22), suggesting that this cleavage site is important for cell tropism in coronaviruses. Previously, we found that QX-type IBV with a mutant S protein containing an extra furin cleavage site named rYN-S2/RRKR infected the CNS of chickens and caused severe encephalitis with obvious neurological symptoms (23).

Here, we further investigated the pathogenesis of neurotropic IBV by real-time quantitative PCR (RT-qPCR) and immunohistochemistry (IHC) to clarify the distribution of viruses in chickens. Blood-brain barrier (BBB) permeability was analyzed by administration of trypan blue and Evans blue and magnetic resonance imaging (MRI). We investigated cell tropism by intracerebral pathogenicity index (ICPI) experiments eliminating interference of the BBB. By infecting chicken embryo primary neuron (CEN) cells, the cell tropism of rYN-S2/RRKR and inhibition of the furin inhibitor were confirmed. The pathogenesis and cell tropism of neurotropic QX-type IBV with an extra FCS were demonstrated. Our findings are a new discovery for γ-CoV and extend our understanding of the function of the S protein of coronavirus.

RESULTS

Disease course of rYN and rYN-S2/RRKR infection. The disease course of rYN-S2/RRKR infection in chickens was compared with that of rYN by clinical signs, immunohistochemistry (IHC) analysis, and viral load examination. Clinical observations indicated that paralysis appeared at 3 days postinoculation (dpi) and that slight respiratory symptoms appeared at 4 dpi in the rYN-S2/RRKR-inoculated group compared with the rYN-inoculated group, indicating the acute form of disease induced by rYN-S2/RRKR.

Immunohistochemistry showed that rYN-S2/RRKR was present in brain tissues at 3 and 5 dpi, whereas rYN was detected in trachea only from 3 dpi (Fig. 1A and B). rYN-S2/RRKR was not detected in the kidney and peripheral nerves during the time course (Fig. 1C and D), suggesting that it crossed the BBB to infect the CNS, and was not transmitted to the CNS by the infected peripheral nerve cells. In tracheas, viruses were detected from 2 dpi and viral loads were higher in the rYN-inoculated group than in the rYN-S2/RRKR-inoculated group at 4 and 5 dpi (Fig. 1E). Viruses were present in the brains of the rYN-S2/RRKR-inoculated group from 3 dpi, and the viral load peaked at 5 dpi, whereas no virus was present in the brains of rYN- or phosphate buffered saline

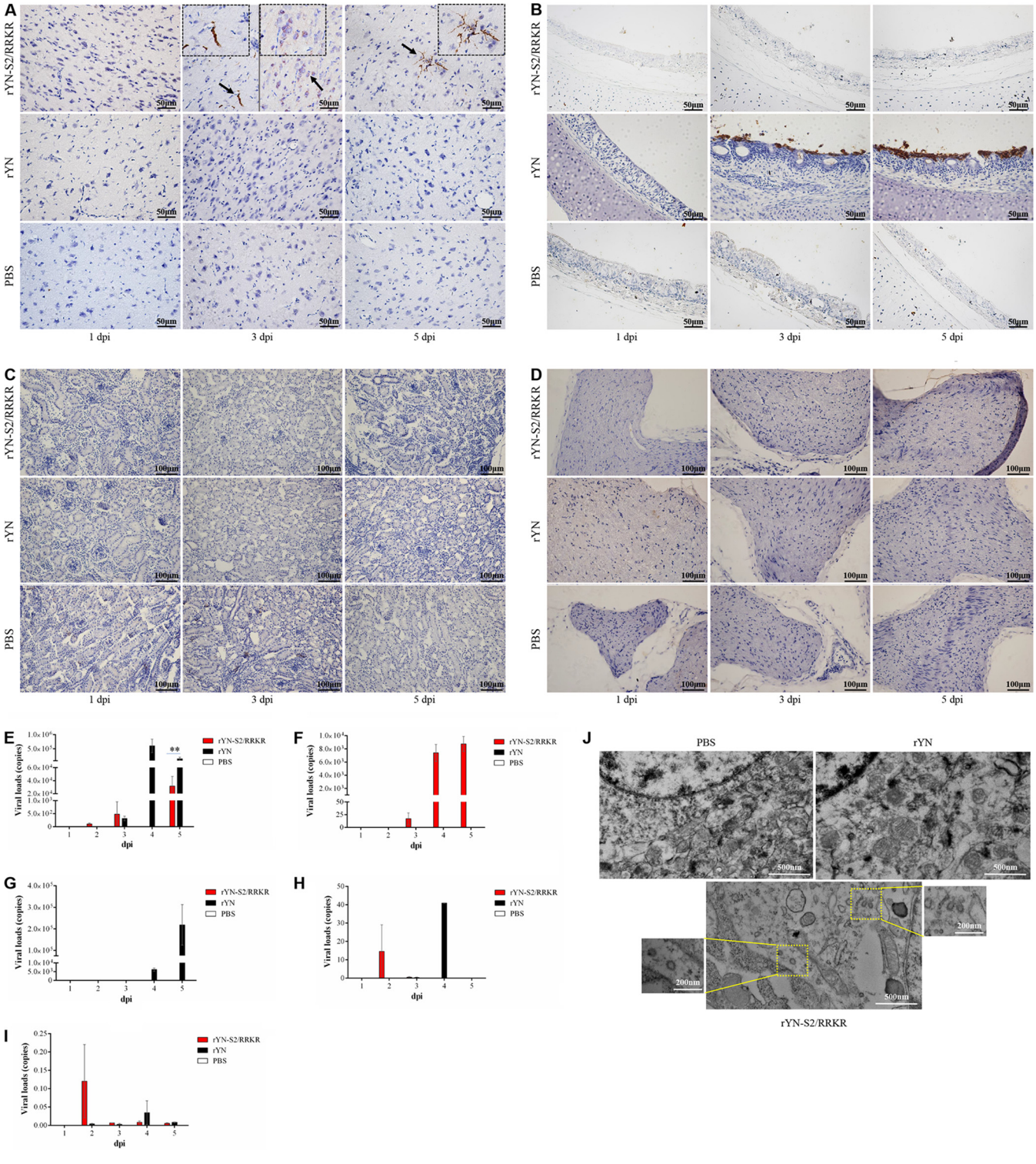

FIG 1 Course of rYN and rYN-S2/RRKR infection. (A) IHC results of brains at 1, 3, and 5 dpi. Only rYN-S2/RRKR was detected in brains, and the N protein of IBV was present in the synapses and cell nuclei. Black arrows indicate IBV-positive neuron cells. (B) IHC results of tracheas at 1, 3, and 5 dpi. rYN was present in the brush border of tracheas at 3 and 5 dpi. (C) IHC results of kidneys at 1, 3, and 5 dpi. No IBV antigen-positive cells were detected in any of the groups. (D) IHC results of peripheral nerves at 1, 3, and 5 dpi. IHC analysis showed that rYN-S2/RRKR and rYN did not infect peripheral nerve cells. (E to I) Viral loads in tracheas (E), brains (F), kidneys (G), lungs (H), and peripheral nerves (I) from 1 to 5 dpi. Viruses were detected in tracheas from 2 dpi, and viral loads in the rYN-inoculated group were higher than those in the rYN-S2/RRKR-inoculated group at 4 and 5 dpi. Viruses were only present in the brains of the rYN-S2/RRKR-inoculated group from 3 dpi, and this reached a peak value at 5 dpi. In the kidneys of the rYN-inoculated group, viruses were first detected at 4 dpi. Very low viral loads were detected in lungs (H) and peripheral nerves (I) by RT-qPCR. **, significant at a P value of $\leq$0.01. (J) TEM observations of brains. Typical coronavirus particles (diameters, 80 to 95 nm) were present in the cytoplasm regions of neuron cells in the rYN-S2/RRKR-inoculated group, but no virus was seen in the brains from the rYN- and PBS-inoculated groups. Magnification, $\times$600 for ICH and $\times$20,000 for TEM.

(PBS)-inoculated groups throughout the disease course (Fig. 1F). There was no viral load in the kidneys of the rYN-S2/RRKR- or PBS-inoculated groups, and virus was not detected until 4 dpi in the rYN-inoculated group, which was significantly later than its appearance in the tracheas (Fig. 1G). RT-qPCR demonstrated low viral loads in the lungs and peripheral nerves of all groups (Fig. 1H and I). To further examine rYN-S2/RRKR replication and damage in the brain, we observed the virus particles by transmission electron microscopy (TEM). Typical coronavirus particles (diameter, 80 to 95 nm) were present in the cytoplasm of neuron cells, but no coronavirus particles were observed in the rYN- and PBS-inoculated groups (Fig. 1J).

rYN-S2/RRKR causes rapid monocyte-associated viremia. To explore the transmission characteristics of the mutant virus in the host, viral loads in all groups were detected by RT-qPCR from 1 to 5 dpi. The results revealed no differences between the rYN-S2/RRKR- and rYN-inoculated groups, suggesting that both parent and mutant viruses were able to cause viremia (Fig. 2A). We prepared blood smears from the anticoagulant blood obtained on 1, 3, and 5 dpi and analyzed them using IHC. rYN-S2/RRKR specifically infected monocytes on 3 and 5 dpi but not red blood cells or heterophilic cells, indicating that it passed through the respiratory epithelial barrier into the bloodstream within 3 days (Fig. 2B). However, rYN was not detected in the blood smears, suggesting its possible extracellular location. To investigate whether monocytes are susceptible to rYN-S2/RRKR, purified mononuclear cells (including monocytes) were infected with rYN-S2/RRKR or rYN. The immunofluorescence results showed that rYN-S2/RRKR did infect monocytes, a result confirmed by the typical nuclear shape, whereas rYN did not infect monocytes (Fig. 2C). Collectively, these results indicate that rYN-S2/RRKR induces a rapid monocyte-associated viremia in the host.

rYN-S2/RRKR infection increases the BBB permeability. After infection of the CNS, we analyzed the permeability of the BBB by MRI at 2 dpi in chickens without clinical symptoms. T_1-weighted images of the brain coronal plane were acquired 10 min after administration of an intravenous contrast medium. Regions of hyperintensity indicated BBB breakdown (Fig. 3A).

The permeability of the BBB was evaluated further after intravenous administration of trypan blue and Evans blue. At necropsy, tissues including the liver and intestinal tract were stained blue in all groups, whereas blue staining of the brain was observed only in the rYN-S2/RRKR-inoculated group. The brain tissues were prepared as paraffin sections for the microscopic observation of trypan blue. Dye particles were present in the brains of the rYN-S2/RRKR-inoculated group, whereas no dye particles were present in the rYN- or PBS-inoculated groups, which was consistent with necropsy (Fig. 3B). Liver paraffin sections were observed by microscopy as a control to ensure that trypan blue was successfully injected (Fig. 3B).

In the Evans blue-inoculated groups, brain tissues of equal weight were added to 1 ml dimethylformamide (DMF) at 60°C for 24 h. The optical density (OD) values of the supernatant at 620 nm were detected, and the concentrations of Evans blue were calculated according to a standard curve (Fig. 3C). The Evans blue content of the rYN-S2/RRKR-inoculated group was higher than that of the rYN- and PBS-inoculated groups, which had similar Evans blue contents of almost 0 (Fig. 3D). These results indicate that rYN-S2/RRKR increased the permeability of the BBB, as indicated by dye particles in the brain.

Intravenous administration of rYN-S2/RRKR is important for the effective crossing of the BBB. Clinical observations showed two dead chickens in the rYN-S2/RRKR intraocularly inoculated group at 4 dpi (mortality rate, 20%). Although the development of disease in the rYN-S2/RRKR intravenously inoculated group was delayed (depression and paralysis at 7 dpi), all the diseased chickens died at 9 dpi (mortality rate, 80%). In the rYN intraocularly inoculated group, two chickens died at 11 dpi with mottled and swollen kidneys (mortality rate, 20%). There were no diseased or dead chickens in the rYN intravenously inoculated group (Fig. 4A).

rYN lacking a furin-S2′ site does not infect neuron cells. (i) ICPI. We performed an intracerebral pathogenicity index (ICPI) experiment to evaluate the direct infection

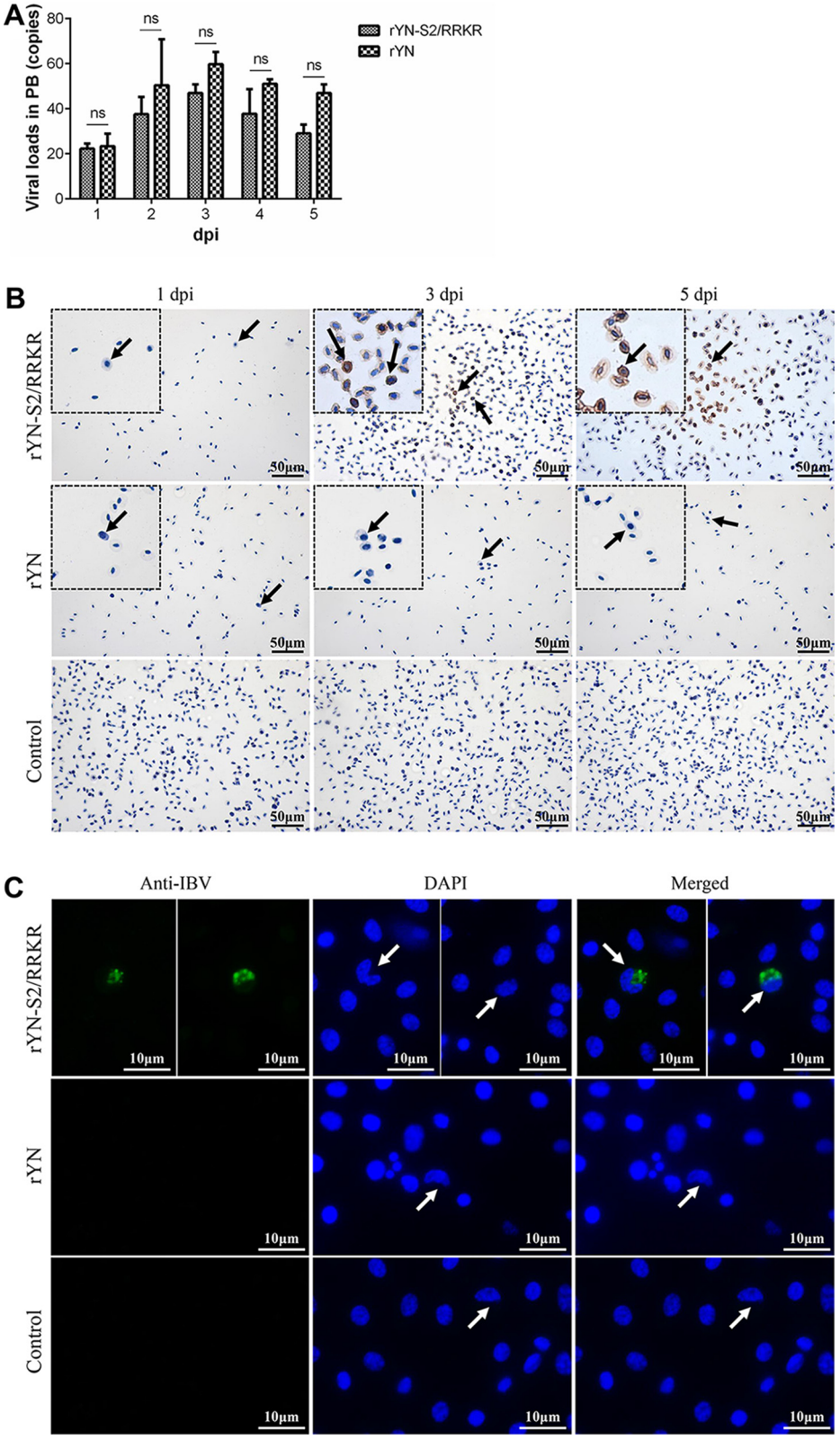

FIG 2 Monocyte-associated viremia caused by rYN-S2/RRKR infection. (A) Viral loads in the PB were measured by RT-qPCR, and no differences were found between the rYN and rYN-S2/RRKR groups, revealing that rYN and rYN-S2/RRKR can both cause viremia. ns, nonsignificant. (B) The IHC results for the blood smears showed that rYN-S2/RRKR specifically infected monocytes (magnification, ×600) on 3 and 5 dpi but not red blood cells or heterophilic cells. (C) Immunofluorescence staining of monocytes. rYN does not infect monocytes. Black and white arrows indicate monocytes in the peripheral blood (magnification, ×1,000).

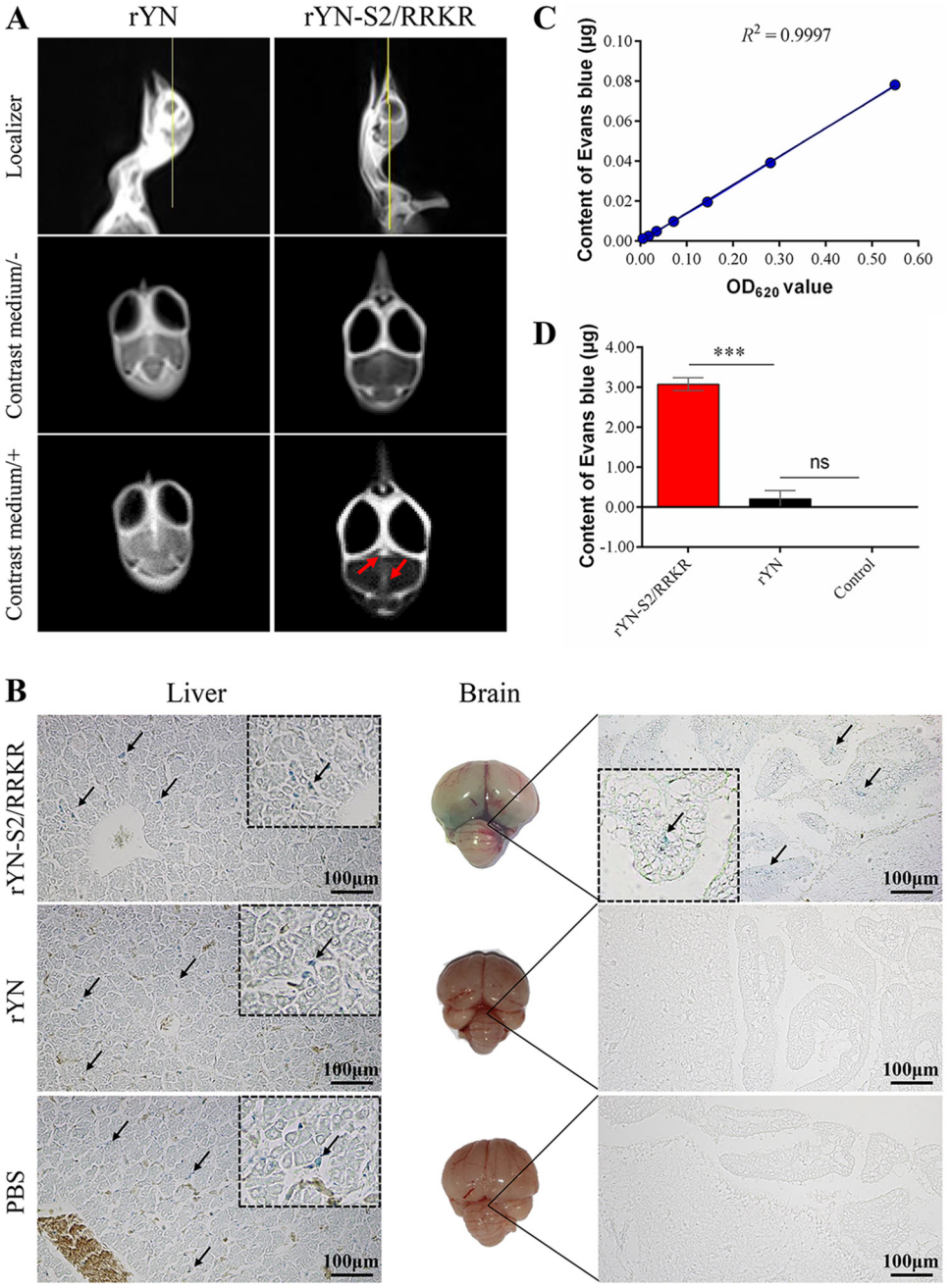

FIG 3 Blood-brain barrier permeability evaluation. (A) MRI analysis at 2 dpi. T_1-weighted images of the brain coronal plane were acquired 10 min after intravenous administration of a contrast medium. The region of hyperintensity indicated increased BBB permeability in the rYN-S2/RRKR-inoculated group. Red arrows indicate contrast medium in the brain. (B) Results of necropsy and paraffin sections. Blue-stained brains and dye particles in brain sections were noted in the rYN-S2/RRKR-inoculated group. Dye particles were observed in all liver paraffin sections of all groups, showing that trypan blue was injected successfully. (C) Standard curve of Evans blue. Two percent Evans blue solution was serially diluted 2-fold, and the OD_{620} values were measured. (D) Content of Evans blue in brains. Evans blue content of the rYN-S2/RRKR-inoculated group was higher than that in the rYN- or PBS-inoculated groups. ***, extremely significant at a P value of ≤0.001.

capacity of rYN and rYN-S2/RRKR by eliminating interference from the BBB. Diseased chickens were observed at 2 dpi in the rYN-S2/RRKR group with head tremor and paralysis. Eight of 10 chickens died during the observation period (mortality rate, 80%) (Fig. 4B). We scored the disease severity according to the clinical signs with reference to the

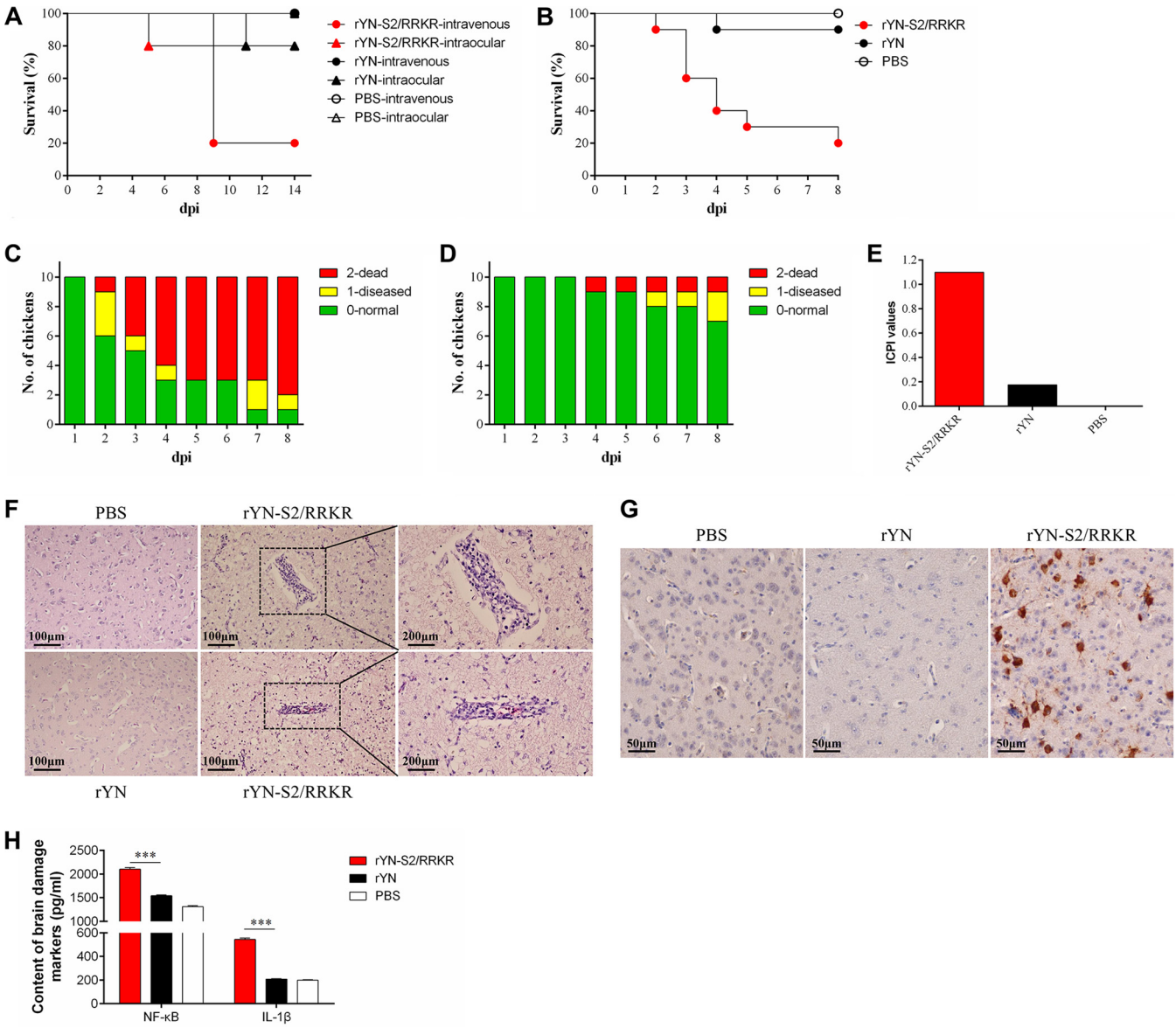

FIG 4 The furin-S2′ site expands cell tropism in IBV and leads to brain damage. (A) Survival of parent and mutant virus groups administered via different inoculation routes. The mortality rate of the rYN-S2/RRKR intravenously inoculated group was highest (80%) among all groups. (B) Survival of ICPI experiments. Disease was observed in chickens in the rYN-S2/RRKR group at 2 dpi, presenting as head tremor and paralysis. Eight of 10 chickens died during the observation period, and the mortality rate was 80%. (C to E) ICPI score. We scored disease with reference to the ICPI guidelines of Newcastle disease virus (NDV) of the Office International des Epizooties (OIE). The ICPI of the rYN-S2/RRKR group was higher than that of the rYN group. (F) Histopathological examination of brain sections. Formation of microglial nodules and perivascular inflammatory infiltrates were observed in the rYN-S2/RRKR group. (G) IHC of brain sections. Many IBV antigen-positive cells were detected in the brains of the rYN-S2/RRKR-inoculated group, and no IBV antigen-positive cells were detected in the rYN-inoculated group. (H) rYN-S2/RRKR leads to brain damage. The expression levels of IL-1β and NF-κB, which are markers of brain damage, were higher in the rYN-S2/RRKR-inoculated group than in the rYN- or PBS-inoculated group. ***, extremely significant at a P value of $\leq$0.001.

ICPI guidelines for Newcastle disease virus (NDV) of the Office International des Epizooties (OIE) (Fig. 4C and D). The ICPI score for the rYN-S2/RRKR group was 1.10 (Fig. 4E). A dead chicken was found at 4 dpi, and two other diseased chickens eventually developed depression in the rYN group (mortality and morbidity rates were 10% and 30%, respectively). The ICPI of the rYN group was 0.175, which was lower than that of the rYN-S2/RRKR group (Fig. 4E). At necropsy, mottled and swollen kidneys were observed in the dead chicken from the rYN group, indicating that rYN mainly damaged the kidneys.

(ii) Histopathological and immunohistochemistry examination. In the ICPI experiment, no microscopic lesions were observed in brains from the rYN and

negative-control groups, whereas microglial nodules and perivascular inflammatory infiltrates were observed in the rYN-S2/RRKR group (Fig. 4F). The results showed that rYN did not cause any injury in the brain even when administered via the intracerebral route. Immunohistochemistry showed that many IBV antigen-positive cells were present in the brains of the rYN-S2/RRKR-inoculated group and that there was no rYN antigen in the brains of the rYN-inoculated group (Fig. 4G). These findings confirmed that the furin-S2′ site is the main factor that determines neuron tropism.

(iii) Brain damage examination. Nuclear factor kB (NF-κB) and interleukin-1β (IL-1β) levels were measured in the brain tissues from all the ICPI experimental groups by ELISA to further verify the brain damage caused by rYN or rYN-S2/RRKR. The results showed that NF-κB and IL-1β expression in the brain tissues from the rYN-S2/RRKR-inoculated group was much higher than that in the rYN- or PBS-inoculated group (Fig. 4H), indicating that rYN does not cause brain damage in its host.

A furin inhibitor prevents virus infection. CEN primary cells were infected with rYN or rYN-S2/RRKR *in vitro*. Laser confocal microscopy showed that rYN-S2/RRKR infected neuron cells, which was prevented in the presence of a furin inhibitor (Fig. 5). Of note, rYN did not infect CEN cells in the presence or absence of the furin inhibitor. These results indicate that the furin-S2′ site has a key role in the neuron tropism of the virus.

rYN-S2/RRKR induces high expression of TNF-α in target tissues and peripheral blood (PB). TNF-α is an important inflammatory cytokine that increases the permeability of the BBB; therefore, we monitored its expression in brains by IHC to investigate how rYN-S2/RRKR crosses the BBB and causes encephalitis. IHC showed that TNF-α was present in microglia and perivascular inflammatory cells in brains from the rYN-S2/RRKR group (Fig. 6A).

Our ELISA results showed that rYN-S2/RRKR induced high levels of TNF-α at 2 dpi in PB and that TNF-α levels returned to normal at 5 dpi, which might increase the permeability of the BBB. In contrast, TNF-α levels in the rYN-inoculated group were similar to those in the PBS-inoculated group at all time points (Fig. 6B). We also measured the levels of the BBB permeability-related myelin basic protein (MBP) in the blood by ELISA. The results showed that MBP content increased at 3 dpi, which was later than that seen for TNF-α. The higher content of MBP was maintained in the PB until 5 dpi (Fig. 6C), indicating that TNF-α is important for rYN-S2/RRKR pathogenicity and contributes to increased BBB permeability.

DISCUSSION

The results of this study provide a detailed explanation for neurotropic IBV that furthers our previous findings with respect to differences in the infection process between rYN-S2/RRKR and rYN, especially the role of the furin-S2′ site in cell tropism. Virulent QX-type IBV with a furin-S2′ site induced severe encephalitis by crossing the BBB, which has not previously been reported. Using ICPI experiments, we confirmed that rYN-S2/RRKR crossed the BBB and infected neuron cells directly. We demonstrated the processes involved in parent and mutant IBV infection. First, rYN-S2/RRKR and rYN infected the trachea. However, at 3 dpi, rYN-S2/RRKR was present in the brain but not in other tissues, as assessed by RT-qPCR and immunohistochemistry. This indicated that rYN-S2/RRKR rapidly infected tracheal epithelial cells and then invaded the brain via the PB. There were high viral loads of rYN in the trachea, but rYN was not detected in kidneys by immunohistochemistry during the experiment, indicating that it took longer to invade the kidneys than the trachea. This difference may be related to RT-qPCR being more sensitive than IHC and shows that the IHC results were probably negative when the RT-qPCR results were positive (Fig. 1C and G). In addition, the results of the IHC and RT-qPCR assays were likely influenced by sample collection in that different viral loads can occur in different parts of the same tissue type. Hence, viral nucleic acid would have been easier to detect than protein in this situation. These findings suggest that the furin-S2′ site was responsible for the acute disease without nephritis caused by rYN-S2/RRKR in comparison with the parent rYN.

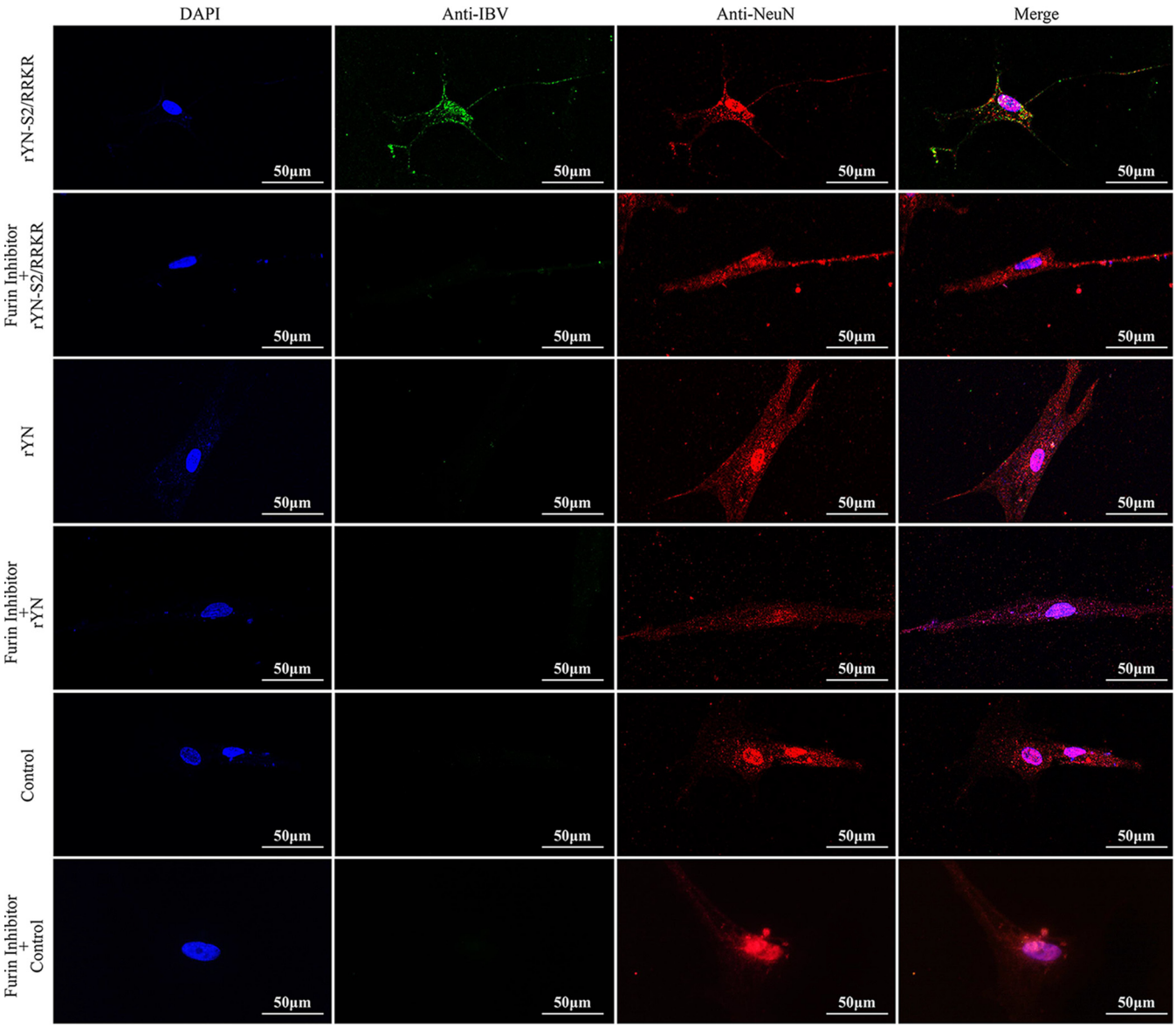

FIG 5 Immunofluorescence staining of CEN cells. Furin inhibitor (FI) prevented rYN-S2/RRKR infection. In contrast, rYN did not infect CEN cells.

MRI demonstrated that the permeability of the BBB was increased at 2 dpi without any clinical symptoms in the rYN-S2/RRKR-inoculated group. The trypan blue and Evans blue experiments also showed that the permeability of the BBB was enhanced by rYN-S2/RRKR, which extends our previous findings (23). Combined with the results of RT-qPCR and immunohistochemistry described above, we confirmed that rYN-S2/RRKR did not infect peripheral neuron cells and, therefore, was not transported to axons in the CNS via the mechanism used by alphaherpesviruses, which infect the CNS, causing encephalitis (24–26). rYN-S2/RRKR infected the CNS immediately by crossing the BBB, and the clinical neurological signs, including paralysis and head tremor, were caused by CNS injury without peripheral neuron cell damage.

The inoculation route might affect the efficiency of infection. When administered by the intraocular route, virus enters the nasal cavity, avoiding the BBB by infecting olfactory cells first and then entering the brain along the olfactory nerve pathway (27–29). This infection route may be rapid, but it is insufficient to cause death. However, virus injected via the intravenous route directly infected monocytes in the

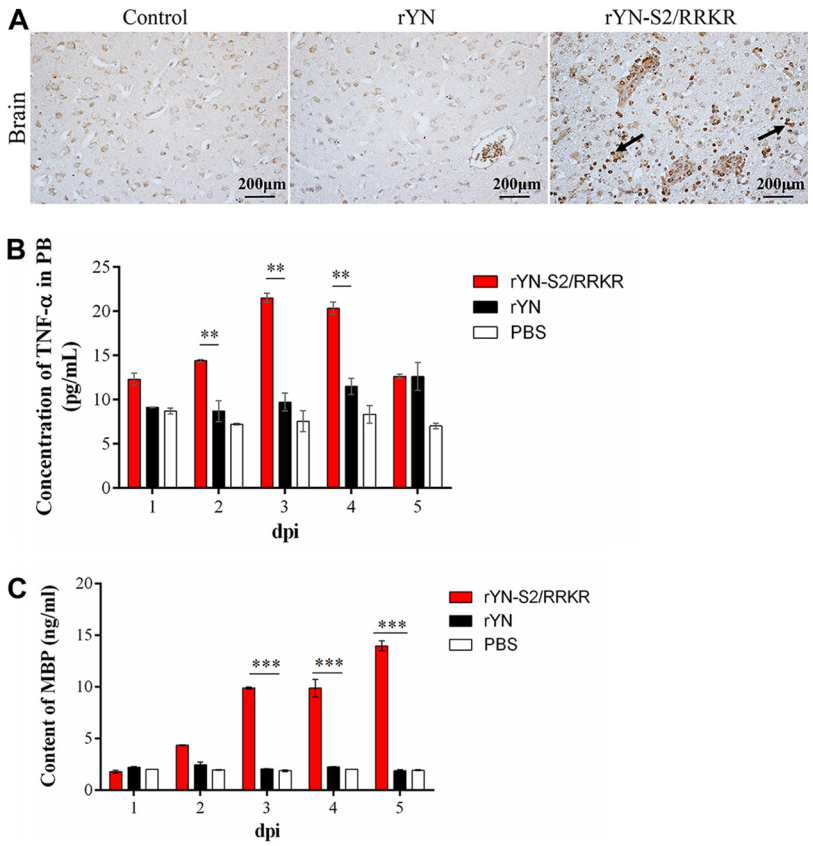

FIG 6 TNF-α contributes to brain infection. (A) TNF-α expression in brains. The results of IHC showed the presence of TNF-α antigen in microglia and perivascular inflammatory cells in brains from the rYN-S2/RRKR group. (B) ELISA detection of TNF-α in PB. rYN-S2/RRKR induced high expression of TNF-α in the PB from 2 dpi. The expression of TNF-α in the rYN-inoculated group was similar to that in the PBS group at all time points. **, significant at a *P* value of $\leq$0.01. (C) MBP expression in PB. The MBP content in PB increased from 3 dpi onwards in the rYN-S2/RRKR group. The MBP content in the rYN-inoculated group was similar to that found in the PBS-inoculated group across all time points. ***, extremely significant at a *P* value of $\leq$0.001.

blood, resulting in brain infection. However, this route might be slower than the intraocular route. As for the different inoculation routes used for the rYN group, it was unexpected that rYN would be more virulent when inoculated intraocularly than when inoculated intravenously. We speculate that intravenous inoculation via the wing vein may lead to a stronger immune response, that rYN might be quickly cleared by lymphocytes, and that rYN probably needs to replicate to high enough levels in the tracheal mucosa to break through humoral immunity or to assist in viral immune evasion. Perhaps rYN also infected the kidneys, which led to death via cerebrospinal fluid circulation in the ICPI experiment. Therefore, different inoculation routes might favor different infection mechanisms in the host.

The original viral sequence PRGR/S in the S2 subunit was replaced with RRKR/S by a reverse genetic system, and the rest of the sequence remained the same, including the S1 subunit, which is the receptor binding domain (RBD). We hypothesized that QX-type IBV infects central neuron cells when the BBB permeability is enhanced. According to ICPI and our experiments with primary neuron cell infections, only rYN-S2/RRKR infected neuron cells *in vivo* and *in vitro*, indicating that rYN without furin-S2′ does not infect neuron cells. We speculated that the presence of the furin-S2′ site might change the fusion activity of the spike protein, resulting in a difference in cell tropism. The infection mechanism underlying this needs further investigation. Previous studies have indicated that SARS-CoV-2 infection of human lung cells requires the

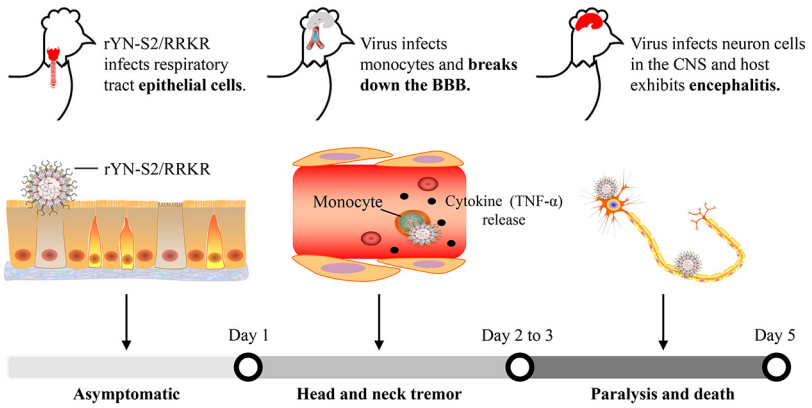

FIG 7 Key phases of disease progression. rYN-S2/RRKR infects epithelial cells in the upper respiratory tract, and the host is asymptomatic. The virus traverses the respiratory epithelial barrier without inducing obvious damage, infects monocytes, causing viremia, and enhances the permeability of the BBB. Finally, the host develops encephalitis.

proteolytic activation of the S protein at the furin cleavage site that is present in almost all clinical SARS-CoV-2 isolates but absent from SARS-CoV (30, 31). The furin cleavage site might expand SARS-CoV-2 cell tropism and facilitate its transmission from wild animals to humans, similar to that suggested after recombination with bat coronaviruses (32). Neuropilin 1 (NRP1), a receptor that binds the "R-X-X-R" motif in the spike protein that is exposed after furin cleavage, enabled SARS-CoV-2 cell entry and provided a direct route to the brain (33).

Our results indicate that modification of the S protein upstream of the FP by furin was essential for QX-type virus to increase the permeability of the BBB by inducing high TNF-α expression, which might be related to the infection of monocytes. TNF-α is related to the increased permeability of the BBB (34–36). It activates TNF receptor 2 (TNFR2) localized on the vascular endothelium to cause the acute breakdown of the blood-cerebrospinal fluid barrier (B-CSF-B) and delayed breakdown of the BBB (37). In addition, activated microglia release matrix metalloproteinase (MMP), which degrades the basement membrane and changes the expression and distribution of claudins breaking the BBB (38, 39).

Outbreaks of coronaviruses have occurred three times in 2 decades, and further research is required. The FCS insertion caused the SARS-CoV-2 pandemic in humans, and an extra FCS in the S2′ site of avian coronavirus increased the cell types infected from epithelial cells to neurons. IBV, a respiratory virus, first entered cells lining the respiratory tract, but when harboring a furin-S2′ site, it broke the respiratory epithelial barrier without obvious damage, infected monocytes, and enhanced the permeability of the BBB, causing encephalitis (Fig. 7). This suggests that the FCS has a key role in virus pathogenicity, especially for coronaviruses.

In summary, we identified the process of disease and a new cell type tropism caused by avian coronavirus with a furin-S2′ site. Viral N protein was detected in the brains and monocytes in blood from infected chickens, suggesting that avian coronavirus with a furin-S2′ site infects the host brain. These results provide insight into the neurological manifestations of other coronaviruses, including HCoV-OC43 and SARS-CoV-2. A previous study confirmed that SARS-CoV-2 infected neurospheres and brain organoids, suggesting that it can infect the human brain (40). However, the permeability of the BBB was not evaluated in that study. Here, we demonstrated that avian coronavirus with a furin-S2′ site increased the permeability of the BBB *in vivo*. The question remains, why does QX-IBV with a furin-S2′ site with the same RBD as the parent strain bind to monocytes and neuron cells? The receptor of the mutant S protein and the mechanism of brain damage will be explored in target tissues and cells in our future study.

MATERIALS AND METHODS

Cells and viruses. Chicken embryo primary neuron (CEN) cells were generated from 18-day-old specific-pathogen-free (SPF) chicken embryos to measure the infectious capacity of rYN and rYN-S2/RRKR *in vitro*. Chicken embryo brain tissues isolated from 18-day-old SPF chicken embryos were digested with 0.25% trypsin at 37°C for 10 min and cultured in Dulbecco's modified Eagle medium (DMEM; Thermo Fisher, Waltham, MA, USA) supplemented with 10% fetal bovine serum (FBS) under 5% CO_2 at 37°C. After the 24-h cultures, the medium was changed to Neurobasal A medium (Thermo Fisher) with 1% penicillin, 1% streptomycin, 2% B27, and 2 mM L-glutamine. Then, 2 mM Ara-C was added to the culture on the third day to restrain the growth of nonneuronal cells. CEN cells were treated with or without furin inhibitor I (10 μM; Sigma, St. Louis, MO, USA) for 30 min and then were infected with $10^{5.0}$ 50% egg infective doses (EID_{50}) of rYN or rYN-S2/RRKR. The mononuclear cells (including monocytes) that we prepared from vein anticoagulant blood using a chicken PB monocyte separation kit (Solarbio, Beijing, China) were cultured in RPMI 1640 (Thermo Fisher) containing 10% FBS with 5% CO_2 at 37°C. These mononuclear cells were infected with $10^{5.0}$ EID_{50} of rYN or rYN-S2/RRKR. rYN is an infectious molecular clone of the QX-type IBV YN strain, which grows in chicken embryo kidney (CEK) cells. rYN-S2/RRKR is an infectious molecular clone of the IBV-YN strain in which the PRGR/S sequence upstream of the FP has been replaced with RRKR/S (furin-S2′ site).

Animals and ethical statement. All SPF chickens and SPF embryonated eggs were purchased from Beijing Boehringer Ingelheim Vital Biotechnology Co., Ltd. (Beijing, China). All chickens were raised in isolators at the China Agricultural University throughout the experiments with food and water provided *ad libitum*. The treatment of all laboratory animals was approved by the Beijing Administration Committee of Laboratory Animals under the leadership of the Beijing Association for Science and Technology (approval no. SYXK [Jing] 2018-0038). The protocols of this experiment were performed according to the guidelines of the Animal Welfare and Ethical Censor Committee at the China Agricultural University (CAU approval no. 20086).

Disease course of rYN and rYN-S2/RRKR infection. Thirty 1-day-old SPF chickens were randomly divided into three groups of 10 chickens each and kept in three isolators. Two of the three groups were inoculated with 100 μl of rYN or rYN-S2/RRKR strain containing $10^{5.0}$ EID_{50} via the intraocular route. The third group was inoculated with 100 μl of phosphate-buffered saline (PBS) as a negative control. Two chickens from each group were sacrificed at 1, 2, 3, 4, and 5 days postinoculation, and samples of brain, trachea, lung, kidney, and sciatic nerve were stored in 10% neutral formalin for immunohistochemical analyses.

Blood-brain barrier permeability evaluation. Thirty 1-day-old SPF chickens were randomly divided into three groups of 10 chickens each and kept in three isolators. Two of the three groups were inoculated with 100 μl of the rYN or rYN-S2/RRKR strain containing $10^{5.0}$ EID_{50} via the intraocular route. The third group was inoculated with 100 μl of phosphate-buffered saline (PBS) as a negative control. When neural or respiratory symptoms were observed, 100 μl of 1% trypan blue or 2% Evans blue was inoculated via intravenous injection, with five chickens in each group. Chickens were sacrificed at 1 day after trypan blue or Evans blue administration. Brains from the trypan blue-inoculated group were stored in 10% neutral formalin for paraffin sections and brains from the Evans blue-inoculated group were stored in 1 ml dimethylformamide (DMF) at 60°C for 24 h. The OD values at 620 nm (OD_{620}) of supernatants were measured.

Histopathology and IHC. Tissues were collected as described above and immersed in 10% neutral formalin for 48 h. Fixed samples were processed, embedded in paraffin wax, and cut into 5-μm sections for immunohistochemistry (IHC). Sections were subjected to antigen retrieval and blocked by 10% normal goat serum in PBS for 30 min to eliminate nonspecific binding. Tissue sections were then incubated with mouse anti-IBV IgG and TNF-α antibody (Proteintech, Chicago, IL, USA) at a 1:500 dilution in PBS for 12 h at 4°C. They were then incubated with horseradish peroxidase-conjugated rabbit anti-mouse IgG (Sigma) for 1 h. The reaction was visualized using 3,3-diaminobenzidine (DAB; Sigma) for 10 min. Finally, sections were counterstained with hematoxylin and examined by light microscopy. Sections of brain were stained with hematoxylin and eosin and examined by light microscopy for lesions.

IBV detection by real-time quantitative PCR (RT-qPCR). Samples from brains, tracheas, lungs, kidneys, sciatic nerves, and anticoagulant blood were collected on 1, 2, 3, 4, and 5 dpi. RNA was extracted from the samples using a Total RNA isolation kit (FORE GENE, Chengdu, China). The viral loads were determined with a Light Cycler 96 real-time PCR system as described previously (41).

TEM. Brains were removed under strict aseptic conditions, cut into slices, immersed in 2% paraformaldehyde and 2.5% glutaraldehyde in 0.1 M phosphate buffer (pH 5.5), and fixed for 2 h at 4°C. After primary fixation, samples were washed with PBS, postfixed in 1% osmium tetroxide, washed, and dehydrated in an increasing series of ethanol solutions. Dehydrated pellets were embedded in an epoxy resin, and sections were cut at 70 nm. Finally, sections were placed on copper sieves and stained with uranyl acetate and lead citrate. Sections were imaged using a JEM-1230 transmission electron microscope (TEM) (JEOL, Tokyo, Japan).

MRI analysis. Magnetic resonance images (MRI) were acquired using a 0.3T quality image QI-V3000 (Shenzhen Cutting-Edge Technology Co., Ltd). Spin-echo T_1-weighted images (repetition time [TR], 110 ms; echo time [TE], 16 ms) were acquired before contrast medium injection and 10 min after contrast medium injection to achieve image enhancement related to BBB permeability. The slice thickness was 3 mm for coronal images.

Effect of different inoculation routes on pathogenicity. Sixty 2-week-old SPF chickens were divided at random into six groups of 10 chickens each and kept in six isolators. Two of the six groups were inoculated with 100 μl of the rYN or rYN-S2/RRKR strain containing $10^{5.0}$ EID_{50} via the intraocular route.

Two other groups were intravenously inoculated with 100 μl of the rYN or rYN-S2/RRKR strain. The final two groups were inoculated with 100 μl of PBS via the intraocular and intravenous routes as negative-control groups.

ICPI. Thirty 1-day-old SPF chickens were divided at random into three groups of 10 chickens each and kept in three isolators. Two of these three groups were inoculated with 50 μl of the rYN or rYN-S2/RRKR strain containing $10^{5.0}$ EID_{50} via the intracerebral route. All chickens were observed for 8 days and evaluated using a ranked score of 0, 1, and 2. These scores represented the following: 0, normal; 1, diseased; and 2, dead. The intracerebral pathogenicity index (ICPI) of rYN and rYN-S2/RRKR was calculated as described previously for the ICPI of NDV.

Immunofluorescence staining. CEN cells were prepared with Immunol staining fix solution, immunostaining permeabilization buffer with Triton X-100, and QuickBlock blocking buffer for Immunol staining (Beyotime Biotechnology, Beijing, China) for 15 min at room temperature. Cells were then incubated with mouse anti-IBV (1:1,000; Hytest, Finland) and rabbit anti-NeuN neuronal marker (1:1,000; Abcam, USA) for 12 h at 4°C. After washing three times in PBS, cells were incubated with anti-mouse IgG(H+L), $F(ab')_2$ fragment (Alexa Fluor 488 conjugate), and anti-rabbit IgG(H+L), $F(ab')_2$ fragment (Alexa Fluor 555 conjugate) (Cell Signaling Technology, Danvers, MA, USA), for 1 h at 37°C. The mononuclear cells, which were prepared as described above, were incubated with mouse anti-IBV (1:1,000; Hytest) and $F(ab')_2$ fragment (Alexa Fluor 488 conjugate). The cells were stained with DAPI (Sigma) for 5 min at room temperature to determine the shapes of the cell nuclei.

Detection of TNF-α and MBP in serum. Serum was collected from 1 to 5 dpi, and the levels of TNF-α and MBP were determined using a chicken TNF-α ELISA kit and chicken MBP ELISA kit (Dogesce, Beijing, China) in accordance with the manufacturer's instructions. A standard curve was generated by plotting the mean OD (450 nm) obtained for each of the six standard concentrations on the *x* axis versus the corresponding concentration on the *y* axis to determine the amount of TNF-α and MBP in the serum.

Detection of brain-specific NF-κB and IL-1β levels. Brains of equal weights were collected from chickens in the ICPI experiments. NF-κB and IL-1β levels in the brain grinding fluid were determined using a chicken NF-κB ELISA kit and a chicken IL-1β ELISA kit (Dogesce) according to the manufacturer's instructions. A standard curve was generated by plotting the mean OD (450 nm) obtained from each of the six standard concentrations on the *x* axis versus the corresponding concentration on the *y* axis to determine the amount of brain-specific TNF-α and MBP.

ACKNOWLEDGMENTS

This work was supported by grant no. 2018YFD0500106 from the National Key Research and Development Program of China.

We thank J. Ludovic Croxford and Sandra Cheesman from Liwen Bianji, Edanz Group China (https://www.liwenbianji.cn/ac), for editing the English text of a draft of this manuscript. We are grateful to C. Xiong and G. Tang in Meilianzhonghe Veterinary Hospital for performing anesthesia and MRI on the chickens.

REFERENCES

1. Peiris JSM, Lai ST, Poon LLM, Guan Y, Yam LYC, Lim W, Nicholls J, Yee WKS, Yan WW, Cheung MT, Cheng VCC, Chan KH, Tsang DNC, Yung RWH, Ng TK, Yuen KY. 2003. Coronavirus as a possible cause of severe acute respiratory syndrome. Lancet 361:1319–1325. https://doi.org/10.1016/S0140-6736(03)13077-2.
2. Zaki AM, van Boheemen S, Bestebroer TM, Osterhaus ADME, Fouchier RAM. 2012. Isolation of a novel coronavirus from a man with pneumonia in Saudi Arabia. N Engl J Med 367:1814–1820. https://doi.org/10.1056/NEJMoa1211721.
3. Li Q, Guan X, Wu P, Wang X, Zhou L, Tong Y, Ren R, Leung KSM, Lau EHY, Wong JY, Xing X, Xiang N, Wu Y, Li C, Chen Q, Li D, Liu T, Zhao J, Liu M, Tu W, Chen C, Jin L, Yang R, Wang Q, Zhou S, Wang R, Liu H, Luo Y, Liu Y, Shao G, Li H, Tao Z, Yang Y, Deng Z, Liu B, Ma Z, Zhang Y, Shi G, Lam TTY, Wu JT, Gao GF, Cowling BJ, Yang B, Leung GM, Feng Z. 2020. Early transmission dynamics in Wuhan, China, of novel coronavirus-infected pneumonia. N Engl J Med 382:1199–1207. https://doi.org/10.1056/NEJMoa2001316.
4. Zhu N, Zhang D, Wang W, Li X, Yang B, Song J, Zhao X, Huang B, Shi W, Lu R, Niu P, Zhan F, Ma X, Wang D, Xu W, Wu G, Gao GF, Tan W, China Novel Coronavirus Investigating and Research Team. 2020. A novel coronavirus from patients with pneumonia in China, 2019. N Engl J Med 382:727–733. https://doi.org/10.1056/NEJMoa2001017.
5. Rabaan AA, Al-Ahmed SH, Haque S, Sah R, Tiwari R, Malik YS, Dhama K, Yatoo MI, Bonilla-Aldana DK, Rodriguez-Morales AJ. 2020. SARS-CoV-2, SARS-CoV, and MERS-COV: a comparative overview. Infez Med 28:174–184.
6. Bergmann CC, Lane TE, Stohlman SA. 2006. Coronavirus infection of the central nervous system: host-virus stand-off. Nat Rev Microbiol 4:121–132. https://doi.org/10.1038/nrmicro1343.
7. St-Jean JR, Jacomy H, Desforges M, Vabret A, Freymuth F, Talbot PJ. 2004. Human respiratory coronavirus OC43: genetic stability and neuroinvasion. J Virol 78:8824–8834. https://doi.org/10.1128/JVI.78.16.8824-8834.2004.
8. Mora-Díaz JC, Piñeyro PE, Houston E, Zimmerman J, Giménez-Lirola LG. 2019. Porcine hemagglutinating encephalomyelitis virus: a review. Front Vet Sci 6:53. https://doi.org/10.3389/fvets.2019.00053.
9. Abdelaziz OS, Waffa Z. 2020. Neuropathogenic human coronaviruses: a review. Rev Med Virol 30:e2118. https://doi.org/10.1002/rmv.2118.
10. Luers JC, Rokohl AC, Loreck N, Wawer Matos PA, Augustin M, Dewald F, Klein F, Lehmann C, Heindl LM. 2020. Olfactory and gustatory dysfunction in coronavirus disease 19 (COVID-19). Clin Infect Dis 71:2262–2264. https://doi.org/10.1093/cid/ciaa525.
11. Reichard RR, Kashani KB, Boire NA, Constantopoulos E, Guo Y, Lucchinetti CF. 2020. Neuropathology of COVID-19: a spectrum of vascular and acute disseminated encephalomyelitis (ADEM)-like pathology. Acta Neuropathol 140:1–6. https://doi.org/10.1007/s00401-020-02166-2.
12. Lahiri D, Mondal R, Deb S, Bandyopadhyay D, Shome G, Sarkar S, Biswas SC. 2020. Neuroinvasive potential of a primary respiratory pathogen SARS- CoV2: summarizing the evidences. Diabetes Metab Syndr 14:1053–1060. https://doi.org/10.1016/j.dsx.2020.06.062.
13. von Weyhern CH, Kaufmann I, Neff F, Kremer M. 2020. Early evidence of pronounced brain involvement in fatal COVID-19 outcomes. Lancet 395:e109. https://doi.org/10.1016/S0140-6736(20)31282-4.
14. Cheng J, Huo C, Zhao J, Liu T, Li X, Yan S, Wang Z, Hu Y, Zhang G. 2018. Pathogenicity differences between QX-like and Mass-type infectious bronchitis viruses. Vet Microbiol 213:129–135. https://doi.org/10.1016/j.vetmic.2017.11.027.

15. Zhong Q, Hu Y-x, Jin J-h, Zhao Y, Zhao J, Zhang G-z. 2016. Pathogenicity of virulent infectious bronchitis virus isolate YN on hen ovary and oviduct. Vet Microbiol 193:100–105. https://doi.org/10.1016/j.vetmic.2016.08.017.
16. Hulswit RJG, de Haan CAM, Bosch BJ. 2016. Coronavirus spike protein and tropism changes. Adv Virus Res 96:29–57. https://doi.org/10.1016/bs.aivir.2016.08.004.
17. Sun Y, Liao Y, Wang H, Tan L, Yuan X, Meng C, Mao X, Song C, Qiu X, Ding C. 2019. Infectious bronchitis virus entry mainly depends on clathrin mediated endocytosis and requires classical endosomal/lysosomal system. Virology 528:118–136. https://doi.org/10.1016/j.virol.2018.12.012.
18. Bosch BJ, van der Zee R, de Haan CAM, Rottier PJM. 2003. The coronavirus spike protein is a class I virus fusion protein: structural and functional characterization of the fusion core complex. J Virol 77:8801–8811. https://doi.org/10.1128/jvi.77.16.8801-8811.2003.
19. Bickerton E, Maier HJ, Stevenson-Leggett P, Armesto M, Britton P. 2018. The S2 subunit of infectious bronchitis virus Beaudette is a determinant of cellular tropism. J Virol 92:e01044-18. https://doi.org/10.1128/JVI.01044-18.
20. Bosch BJ, Bartelink W, Rottier PJM. 2008. Cathepsin L functionally cleaves the severe acute respiratory syndrome coronavirus class I fusion protein upstream of rather than adjacent to the fusion peptide. J Virol 82:8887–8890. https://doi.org/10.1128/JVI.00415-08.
21. Coutard B, Valle C, de Lamballerie X, Canard B, Seidah NG, Decroly E. 2020. The spike glycoprotein of the new coronavirus 2019-nCoV contains a furin-like cleavage site absent in CoV of the same clade. Antiviral Res 176:104742. https://doi.org/10.1016/j.antiviral.2020.104742.
22. Andersen KG, Rambaut A, Lipkin WI, Holmes EC, Garry RF. 2020. The proximal origin of SARS-CoV-2. Nat Med 26:450–452. https://doi.org/10.1038/s41591-020-0820-9.
23. Cheng J, Zhao Y, Xu G, Zhang K, Jia W, Sun Y, Zhao J, Xue J, Hu Y, Zhang G. 2019. The S2 subunit of QX-type infectious bronchitis coronavirus spike protein is an essential determinant of neurotropism. Viruses 11:972. https://doi.org/10.3390/v11100972.
24. Smith G. 2012. Herpesvirus transport to the nervous system and back again. Annu Rev Microbiol 66:153–176. https://doi.org/10.1146/annurev-micro-092611-150051.
25. Chen S-H, Yao H-W, Huang W-Y, Hsu K-S, Lei H-Y, Shiau A-L, Chen S-H. 2006. Efficient reactivation of latent herpes simplex virus from mouse central nervous system tissues. J Virol 80:12387–12392. https://doi.org/10.1128/JVI.01232-06.
26. Fekete R, Cserép C, Lénárt N, Tóth K, Orsolits B, Martinecz B, Méhes E, Szabó B, Németh V, Gönci B, Sperlágh B, Boldogkői Z, Kittel Á, Baranyi M, Ferenczi S, Kovács K, Szalay G, Rózsa B, Webb C, Kovacs GG, Hortobágyi T, West BL, Környei Z, Dénes Á. 2018. Microglia control the spread of neurotropic virus infection via P2Y12 signalling and recruit monocytes through P2Y12-independent mechanisms. Acta Neuropathol 136:461–482. https://doi.org/10.1007/s00401-018-1885-0.
27. Khan AR, Liu M, Khan MW, Zhai G. 2017. Progress in brain targeting drug delivery system by nasal route. J Control Release 268:364–389. https://doi.org/10.1016/j.jconrel.2017.09.001.
28. Lochhead JJ, Thorne RG. 2012. Intranasal delivery of biologics to the central nervous system. Adv Drug Deliv Rev 64:614–628. https://doi.org/10.1016/j.addr.2011.11.002.
29. Kozlovskaya L, Abou-Kaoud M, Stepensky D. 2014. Quantitative analysis of drug delivery to the brain via nasal route. J Control Release 189:133–140. https://doi.org/10.1016/j.jconrel.2014.06.053.
30. Hoffmann M, Kleine-Weber H, Pöhlmann S. 2020. A multibasic cleavage site in the spike protein of SARS-CoV-2 is essential for infection of human lung cells. Mol Cell 78:779–784. https://doi.org/10.1016/j.molcel.2020.04.022.
31. Bestle D, Heindl MR, Limburg H, Van Lam van T, Pilgram O, Moulton H, Stein DA, Hardes K, Eickmann M, Dolnik O, Rohde C, Klenk HD, Garten W, Steinmetzer T, Böttcher-Friebertshäuser E. 2020. TMPRSS2 and furin are both essential for proteolytic activation of SARS-CoV-2 in human airway cells. Life Sci Alliance 3:e202000786. https://doi.org/10.26508/lsa.202000786.
32. Lau SY, Wang P, Mok BWY, Zhang AJ, Chu H, Lee ACY, Deng S, Chen P, Chan KH, Song W, Chen Z, To KKW, Chan JFW, Yuen KY, Chen H. 2020. Attenuated SARS-CoV-2 variants with deletions at the S1/S2 junction. Emerg Microbes Infect 9:837–842. https://doi.org/10.1080/22221751.2020.1756700.
33. Matheson NJ, Lehner PJ. 2020. How does SARS-CoV-2 cause COVID-19? Science 369:510–511. https://doi.org/10.1126/science.abc6156.
34. Sibson NR, Blamire AM, Perry VH, Gauldie J, Styles P, Anthony DC. 2002. TNF-α reduces cerebral blood volume and disrupts tissue homeostasis via an endothelin- and TNFR2-dependent pathway. Brain 125:2446–2459. https://doi.org/10.1093/brain/awf256.
35. Alexander JJ, Jacob A, Cunningham P, Hensley L, Quigg RJ. 2008. TNF is a key mediator of septic encephalopathy acting through its receptor, TNF receptor-1. Neurochem Int 52:447–456. https://doi.org/10.1016/j.neuint.2007.08.006.
36. Tsuge M, Yasui K, Ichiyawa T, Saito Y, Nagaoka Y, Yashiro M, Yamashita N, Morishima T. 2010. Increase of tumor necrosis factor-α in the blood induces early activation of matrix metalloproteinase-9 in the brain. Microbiol Immunol 54:417–424. https://doi.org/10.1111/j.1348-0421.2010.00226.x.
37. Connell JJ, Chatain G, Cornelissen B, Vallis KA, Hamilton A, Seymour L, Anthony DC, Sibson NR. 2013. Selective permeabilization of the blood-brain barrier at sites of metastasis. J Natl Cancer Inst 105:1634–1643. https://doi.org/10.1093/jnci/djt276.
38. da Fonseca ACC, Matias D, Garcia C, Amaral R, Geraldo LH, Freitas C, Lima FRS. 2014. The impact of microglial activation on blood-brain barrier in brain diseases. Front Cell Neurosci 8:362. https://doi.org/10.3389/fncel.2014.00362.
39. Furuse M. 2010. Molecular basis of the core structure of tight junctions. Cold Spring Harb Perspect Biol 2:a002907. https://doi.org/10.1101/cshperspect.a002907.
40. Zhang B-Z, Chu H, Han S, Shuai H, Deng J, Hu Y-F, Gong H-R, Lee AC-Y, Zou Z, Yau T, Wu W, Hung IF-N, Chan JF-W, Yuen K-Y, Huang J-D. 2020. SARS-CoV-2 infects human neural progenitor cells and brain organoids. Cell Res 30:928–931. https://doi.org/10.1038/s41422-020-0390-x.
41. Zhao Y, Cheng J-L, Liu X-Y, Zhao J, Hu Y-X, Zhang G-Z. 2015. Safety and efficacy of an attenuated Chinese QX-like infectious bronchitis virus strain as a candidate vaccine. Vet Microbiol 180:49–58. https://doi.org/10.1016/j.vetmic.2015.07.036.